frontiers in Energy Research

ORIGINAL RESEARCH
published: 11 March 2022
doi: 10.3389/fenrg.2022.810937

Multi-Objective Optimization of a T-Shaped Anti-Sloshing Baffle Based on NSGA-II

Yu Lei[1], *Licheng Zhang*[2], *Shengzhi Zhong*[3] *and Bin Huang*[1]*

[1]Wuhan University of Technology, Wuhan, China, [2]Wuhan Road Rover Intelligent Technology Co., Ltd., Wuhan, China, [3]Liuzhou Wuling Automobile Industry Co., Ltd., Liuzhou, China

Unlike the solid cargo in the truck, the liquid in the tank truck fluctuates with the movement of the vehicle. Most of the current research study focuses on the transverse shock caused by the sloshing liquid and control of the liquid movement in the lateral direction. However, the movement of the fluid in the longitudinal direction also harms the vehicle dynamic. It is caused by the acceleration or deceleration of the truck. To lower the risk, the T-shaped anti-sloshing baffle is designed based on the current research study. To improve the conflict performance of the anti-sloshing baffle, the approximation model and multi-objective optimization method are initiated. The relationship between the anti-sloshing effect and the structural parameters of the anti-sloshing baffle is established by the Kriging method. The NSGA-II is initiated to minimize the maximum pressure caused by the moving liquid and the increasing mass of the anti-sloshing baffle. The maximum pressure is decreased by 40.97%, and the anti-sloshing baffle mass is decreased by 2.77%. With the optimized anti-sloshing baffle, the maximum pressure, waving damping time, and the baffle mass are decreased; the force on the tank walls and baffles is distributed more evenly, and the safety of the truck is improved.

Keywords: anti-sloshing baffle, tank truck, multi-objective optimization, NSGA-II, fluid movement

OPEN ACCESS

Edited by:
Jian Zhao,
Shanghai University of Electric Power, China

Reviewed by:
Scappaticci Lorenzo,
Università degli Studi Guglielmo Marconi, Italy
Antonio Mattia Grande,
Politecnico di Milano, Italy
Vasant Annasaheb Matsagar,
Indian Institute of Technology Delhi, India

***Correspondence:**
Bin Huang
huangbin@whut.edu.cn

Specialty section:
This article was submitted to Process and Energy Systems Engineering, a section of the journal Frontiers in Energy Research

Received: *08 November 2021*
Accepted: *14 February 2022*
Published: *11 March 2022*

Citation:
Lei Y, Zhang L, Zhong S and Huang B (2022) Multi-Objective Optimization of a T-Shaped Anti-Sloshing Baffle Based on NSGA-II. Front. Energy Res. 10:810937. doi: 10.3389/fenrg.2022.810937

INTRODUCTION

Tank trucks are a primary road transportation method of hazardous liquid materials in the world. The tank truck-involved accidents may cause a hazardous material leak which is more harmful than the accident itself. Compared to the truck carrying the solid cargo, the tank trucks are susceptible to rollover due to their size, height of the gravity center, distribution of weight, and the sloshing of liquid in the tank during transportation (Iranitalab et al., 2020). Thus, solving the sloshing problem can improve the safety of the tank truck. There are some researchers in the earthquake areas focusing on the liquid sloshing problem. The properly designed baffle in the vertical tank can reduce the pressure on the tank caused by the sloshing liquid. A suspended annular baffle hanging from the floating roof of cylindrical oil tanks subjected to the earthquake is validated by a scaled experiment (Hosseini et al., 2017). The effect of elastic baffles is also investigated (Zhang et al., 2020). These methods are effective but difficult to be built in the tank truck.

In the tank truck area, some work has been carried out to minimize the liquid sloshing effect. Zhang, J., et al. initiated a numerical model based on the Newtonian Herschel–Bulkley, Bingham equation, and the volume of the fluid method to study the dynamic behavior of a tank with the baffle in the lateral direction (Zhang et al., 2016). Hasheminejad, S. M., et al. used the linear potential theory and conformal mapping technique to develop rigorous mathematical models for transient sloshing

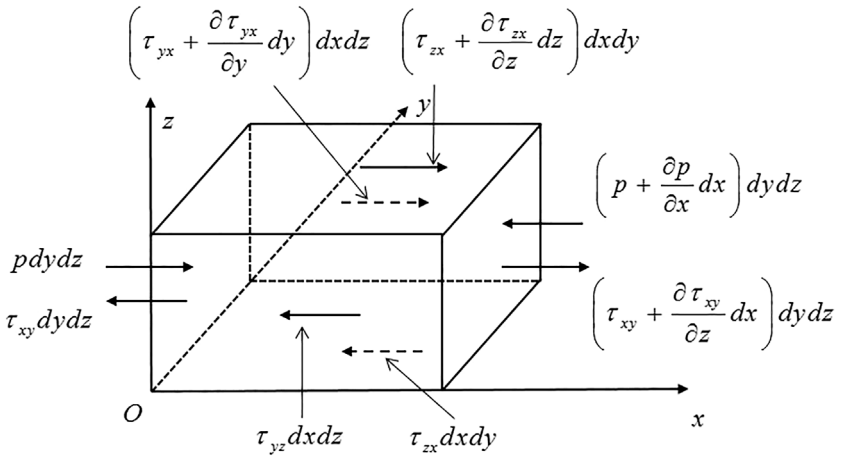

FIGURE 1 | Force analysis of the flow particle in *x* direction.

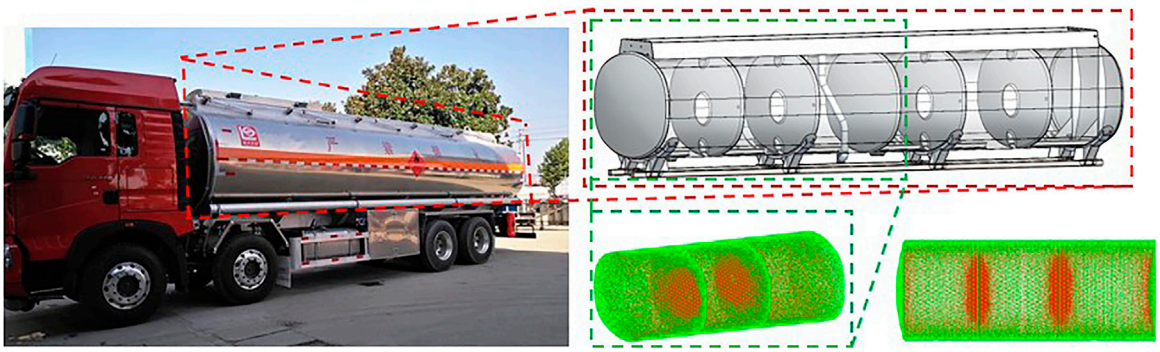

FIGURE 2 | Model of a tank truck.

under a lateral excitation (Hasheminejad et al., 2014). The free surface-touching horizontal side baffles, a central surface-piercing, and a bottom-mounted vertical baffle are considered in their work. Xue, M. A., et al. analyzed the pressure on the tank with four baffles with the experimental method (Xue et al., 2017). The vertical baffle with a four-square perforation has the maximum pressure compared to the tank with the immersed bottom-mounted vertical baffle, vertical baffle flushing with a free surface, and perforated vertical baffle. The influence of the four-square perforation needs to be further analyzed. Akyıldız, H., et al. investigated the liquid sloshing in the cylindrical tank with different ring baffle combination by a scaled experimental method (Akyıldız et al., 2013). The best baffle arrangement is determined by comparing the pressure of the four arrangements. Kolaei, A., et al. built an analytical model to analyze the transient lateral slosh force by the linear slosh theory (Kolaei et al., 2014). In their research, the tank with four different cross sections, circular, elliptical, modified-oval, and Reuleaux triangle are compared; the tanks with a lower overall mass center and critical slosh length have better anti-roll stability. Based on the analytical model, the fluid mass moment in a clean-bore tank, top-mounted baffle, and bottom-mounted baffle are compared to the equivalent rigid cargo. The top-mounted baffle shows the best anti-sloshing ability when the partly filled numbers are 0.8 and 0.92, which are higher than 0.5. The bottom-mounted baffle may be more effective than the top-mounted baffle when the partly filled is lower than 0.5. Compared to the CFD (computational fluid dynamic) method, it can save computation time, but it also needs further research to be initiated in the baffle with a complicated cross section (Kolaei et al., 2017). Wang, W., et al. used a semi-analytical scaled boundary finite-element method (SBFEM) to study the effects of the T-shaped baffle in elliptical tanks (Wang et al., 2016). Three T-shaped baffles are taken into consideration, including surface-piercing, bottom-mounted, and their combined form, and Y-shaped baffles are also included. The parameters of the baffles are associated with the anti-sloshing performance. Xue, M. A., et al. used the virtual boundary force (VBF) method to model the internal baffles of a rectangular tank (Xue and Lin, 2011). The result is validated by the experiment; the effects of ring baffles on

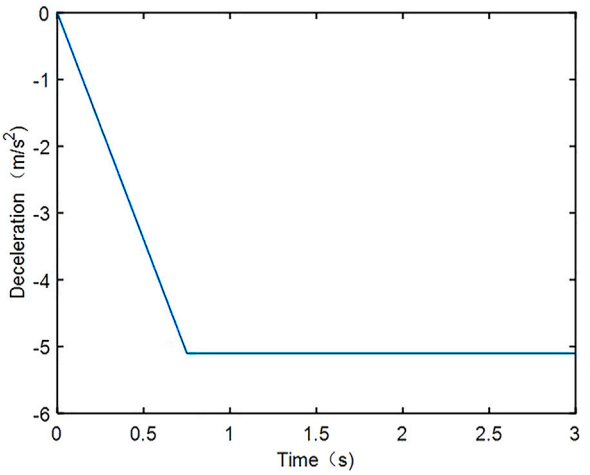

FIGURE 3 | Deceleration varies with the time.

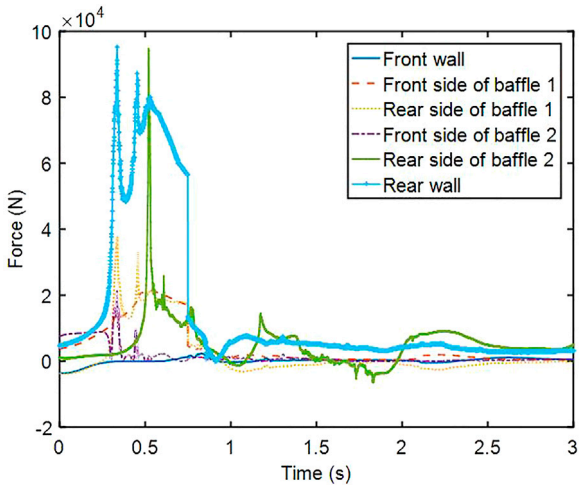

FIGURE 4 | Force on the fluid boundary during the deceleration process.

reducing liquid sloshing are analyzed and discussed. Belakroum, R., et al. provided a method based on an arbitrary Lagrangian–Eulerian (ALE) description of the Navier–Stokes equation (Belakroum et al., 2010). The baffles are mounted on the bottom; the sidewall of a rectangular tank is discussed in their research.

The current research of the tank focuses on lateral excitation, and some new method is used in the analysis of the tank with a simple cross-section baffle. Despite the lateral excitation, the longitudinal movement of the mass center damages also the handling stability (Wan et al., 2019). The CFD method is efficient in this field. Ünal, U. O., et al. carried out the liquid sloshing calculations of rectangular tanks with T-shaped baffles using laminar and turbulent viscous flow solvers (Ünal et al., 2019). The baffle is fully effective in pressure and wave damping when its height is higher than 80% of the liquid level since the tank in this research is fitted with a perforated baffle, which cannot be described by the Q-S model and the pendulum model (Wan et al., 2019). Some commercial platforms are widely used in solving liquid sloshing problems, such as OpenFOAM (Sanapala et al., 2018) and Fluent. The simulation result is validated by the experimental method.

The effect of the ring baffle in the longitudinal direction and the T-shaped baffle in the transverse is proved by the current research study. To investigate the fluid fluctuation process during the acceleration and brake process, the CFD model of the current tank and the tank with a T-shaped baffle in the longitudinal direction is built and analyzed. To improve the anti-sloshing performance and lower the mass of the baffle, the Kriging method and NSGA-II (non-dominated sorted genetic algorithm) are initiated to optimize the parameter of a T-shaped anti-sloshing baffle. According to the comparison of the anti-sloshing performance and the mass of the tank with the current anti-sloshing baffle, the T-shaped baffle before and after optimization and the optimized T-shape baffle have the lowest pressure, force, and mass, which is beneficial to the safety of the tank truck.

THEORY

The movement of the fluid can be described by the continuity equation, momentum equation, and energy equation.

Continuity Equation

The continuity equation is also known as the mass equation which is based on the law of conservation of mass. The mass that flows from the fluid unit equals the decreased mass of the fluid unit. The continuity equation can be impressed as follows:

$$\frac{\partial \rho}{\partial t} + \nabla \cdot (\rho V) = 0. \tag{1}$$

Here, V is the velocity vector of the fluid, and ρ represents the fluid density. When the fluid flow is a steady-state flow and incompressible fluid flow, ρ is a constant value. **Equation 1** can be simplified as follows.

$$\nabla \cdot V = 0. \tag{2}$$

Momentum Equation

The momentum equation is based on the momentum conservation equation. The change rate of the momentum in the fluid unit is caused by the sum of the external force on the fluid volume. The momentum conservation can be written as follows:

$$\frac{\partial (\rho u)}{\partial t} + \nabla \cdot \left(\rho u \vec{V}\right) = -\frac{\partial p}{\partial x} + \frac{\partial \tau_{xx}}{\partial x} + \frac{\partial \tau_{yx}}{\partial y} + \frac{\partial \tau_{zx}}{\partial z} + \rho f_x, \tag{3}$$

$$\frac{\partial (\rho v)}{\partial t} + \nabla \cdot \left(\rho v \vec{V}\right) = -\frac{\partial p}{\partial y} + \frac{\partial \tau_{xy}}{\partial x} + \frac{\partial \tau_{yy}}{\partial y} + \frac{\partial \tau_{zy}}{\partial z} + \rho f_y, \tag{4}$$

$$\frac{\partial (\rho w)}{\partial t} + \nabla \cdot \left(\rho w \vec{V}\right) = -\frac{\partial p}{\partial z} + \frac{\partial \tau_{xz}}{\partial x} + \frac{\partial \tau_{yz}}{\partial y} + \frac{\partial \tau_{zz}}{\partial z} + \rho f_z, \tag{5}$$

where u, v, and w represent the velocity of the fluid in x, y, and z axes, p denotes the pressure, τ_{xx}, τ_{yy}, and τ_{zz} refer to the normal

TABLE 1 | Fluid distribution and pressure during the deceleration process.

Time (s)	Fluid distribution	Pressure
0.35	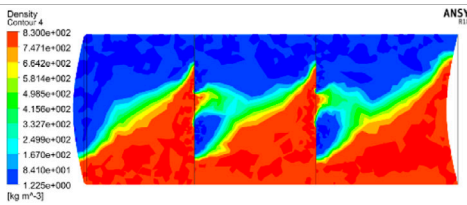	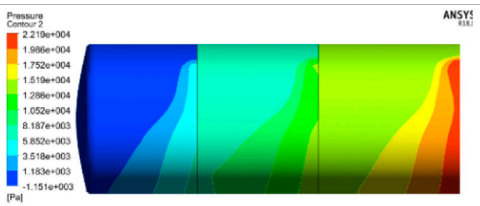
0.40	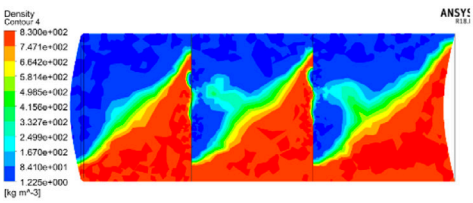	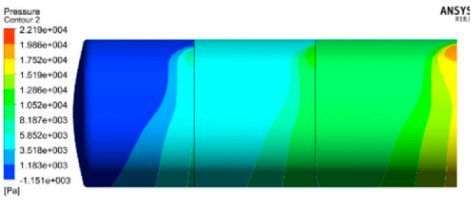
0.45	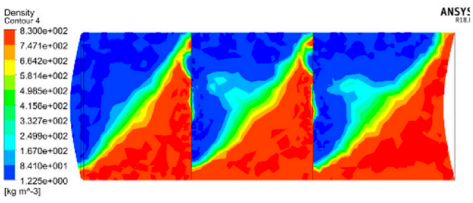	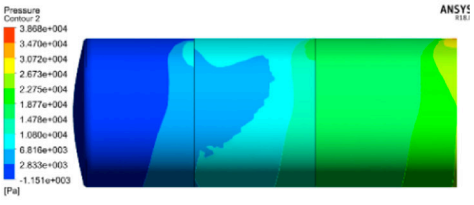
0.50	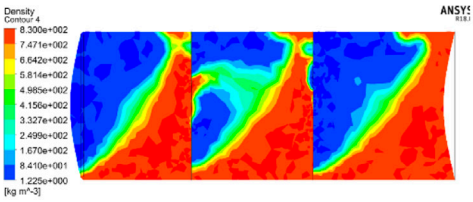	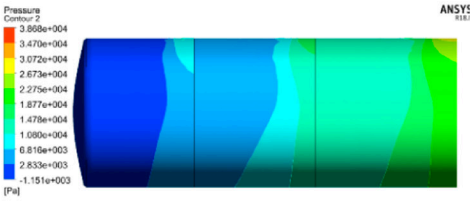
0.55	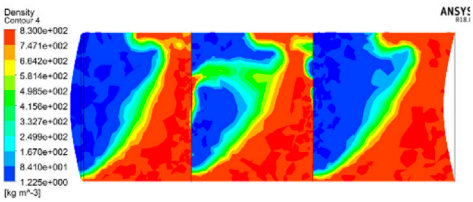	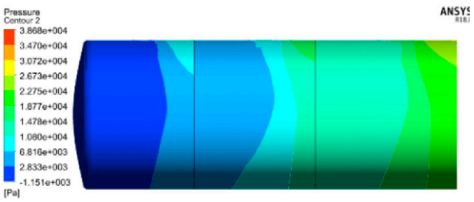
0.60	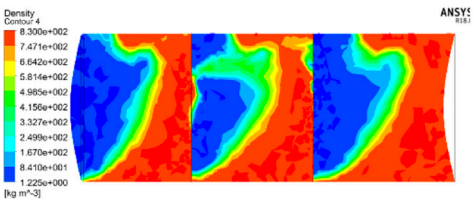	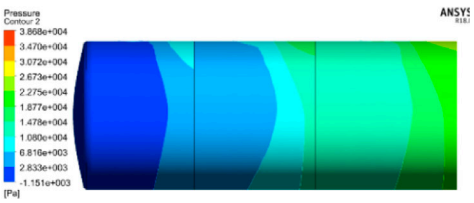

stress while τ_{yx}, τ_{zx}, τ_{xy}, τ_{zy}, τ_{xz}, and τ_{yz} represent shear stress, f_x, f_y, and f_z are the projections of volume force, $\vec{f}$, on the x, y, and z axes.

Energy equation

The energy equation is gained based on the law of conservation of energy. The change rate of the energy in the fluid unit equals the sum of power generated by the force on the fluid unit. The change rate of the energy is made up of two parts: the power caused by the codirectional pressure and speed divergence and the dissipated energy caused by viscosity force (Anderson and Wendt, 1995). The force analysis of the flow particle in the x direction is shown in **Figure 1**

$$\rho\frac{dE}{dt} = -p\left(\frac{\partial v_x}{\partial x} + \frac{\partial v_y}{\partial y} + \frac{\partial v_z}{\partial z}\right) + \tau_{xx}\frac{\partial v_x}{\partial x} + \tau_{yx}\frac{\partial v_x}{\partial y} + \tau_{zx}\frac{\partial v_x}{\partial z} + \tau_{xy}\frac{\partial v_y}{\partial x} + \tau_{yy}\frac{\partial v_y}{\partial y} + \tau_{zy}\frac{\partial v_y}{\partial z} + \tau_{xz}\frac{\partial v_z}{\partial x} + \tau_{zy}\frac{\partial v_z}{\partial y} + \tau_{zz}\frac{\partial v_z}{\partial z}, \tag{6}$$

where E is the interior energy of the fluid unit.

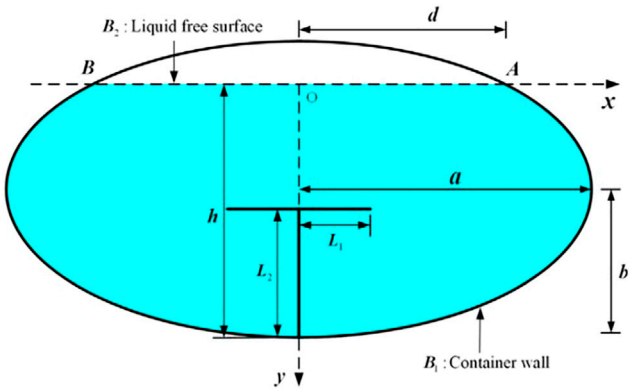

FIGURE 5 | T-shaped baffle in the tank to reduce the fluid movement in the lateral direction.

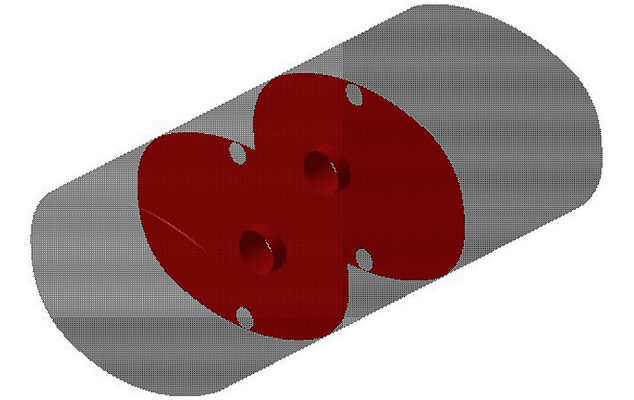

FIGURE 6 | T-shaped anti-sloshing baffle in the tank.

MODEL ESTABLISHMENT

It is difficult to record the movement of the fluid in the tank; therefore, most researchers use scaled transparent tanks to initiate the field test. In Yin Wan's work, the test result of a scaled tank is taken as a reference to validate the CFD model built by Fluent (Wan, 2018).

For the tank truck in this case, the tank is made up of two separate chambers, each of them having two anti-sloshing baffles (baffles 1 and 2, from front to rear of the tank truck), as shown in **Figure 2**. The geometry parameter of the tank is summarized as length, 9,124 mm, width, 2,464 mm, height, 1771 mm, and the radius of the hole, 275 mm.

The layout of the two chambers is the same; therefore, only one chamber is used to establish the CFD model. The boundary of the fluid area is determined based on the tank structure. The established CFD model has 511,125 elements.

The movement of the fluid inside the tank trunk is hard to be determined; therefore, the scaled model with the transparency tank is used in Yin Wan's work to validate the CFD model (Wan et al., 2019). Considering the analysis process of Yin Wan's work as a reference, the VOF (volume of fluid) and transient solver type are set in the CFD model. The Reynolds number for this case is bigger than 2,320; thus, the standard $k-\omega$ model is chosen to solve the turbulence problem. The oil is chosen as the fluid during the analysis. Since the maximum force and pressure usually occur when the fluid degree of filling is 0.5 (Wan et al., 2019), it is chosen as the boundary condition to acquire the most crucial condition of the tank. The oil and air region is determined by the fluid degree of filling in the vertical direction. The oil/air phase interaction mechanism is set as evaporation–condensation.

The fluid movement in the longitudinal direction is mainly caused by the acceleration of the truck in this direction. Thus, the acceleration and deceleration processes should be analyzed to determine the boundary condition. For the tank truck, the acceleration $\dot{v}_a$ can be acquired by **Equation 7**.

$$m\dot{v}_a = \frac{T_{tq} i_t \eta_T}{r} - \frac{1}{2} C_d A \rho v_a^2 - mgf. \tag{7}$$

Here, m means truck mass; T_{tq}, i_t, η_T, and r are engine torque, transmission ration, transmission coefficient, and tire radius; C_d, A, ρ, and v_a present the air drag coefficient, projection area in the longitudinal direction, air density, and speed; and f is the rolling coefficient, respectively.

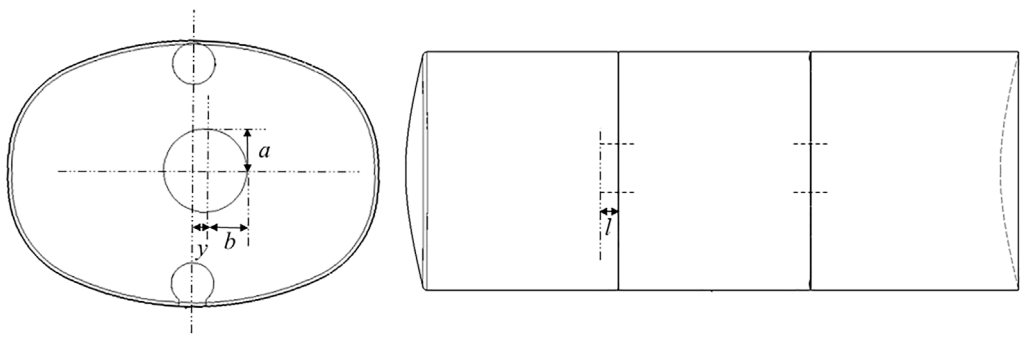

FIGURE 7 | Parameters of the T-shaped anti-sloshing baffle.

TABLE 2 | Error analysis of the approximation model.

Objectives	R^2	RMSE	MAPE (%)
Maximum pressure	0.98	499 Pa	7.74
Mass	0.91	1.15 kg	3.12

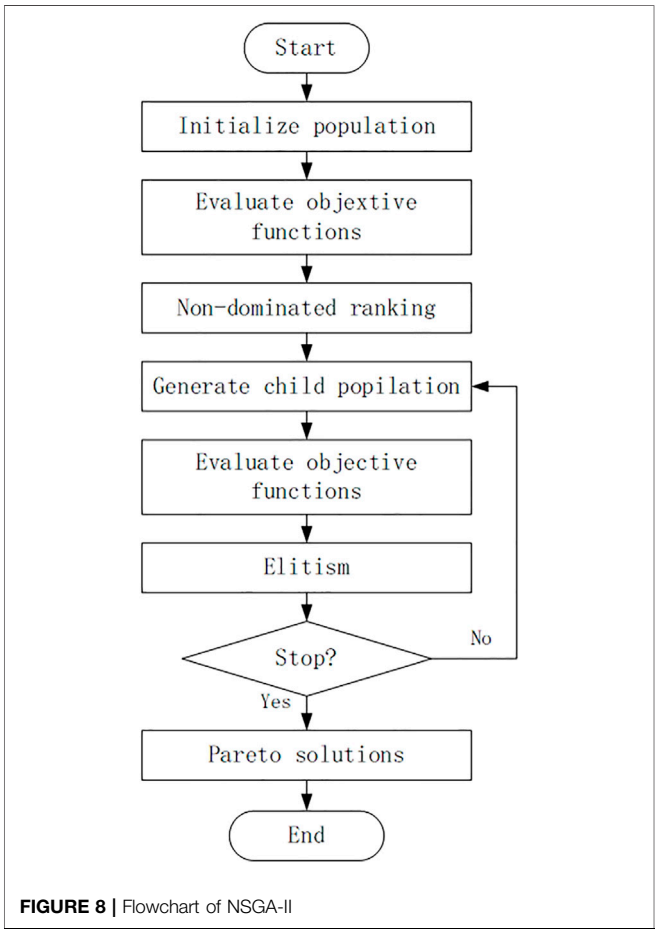

FIGURE 8 | Flowchart of NSGA-II

For the deceleration ability, the truck should satisfy some regulations. Since the tank truck is an N3 vehicle, according to the regulation in ECE R13 (NoRegulation, 2009) and GB 12676-1999 (Liu, 1999) in China, the distance during the brake process from the beginning to end of the brake can be acquired by the following equation.

$$s = 0.15v_d + \frac{100}{25} \times \frac{v_d^2}{115}. \tag{8}$$

Here, s is the maximum brake distance, v_d is the velocity at the beginning of the brake process; for the tank truck, the values of these parameters are 19 m and 50 km/h, respectively.

$$\dot{v}_d = \frac{dv_d}{dt}. \tag{9}$$

According to **Equation 9**, the calculated deceleration $\dot{v}_d$ is 5.08 m/s^2, which is higher than the maximum acceleration of the truck, v_a. Taking the response time of the brake system into consideration, the bake deceleration in the time domain is shown in **Figure 3**, which is taken as the input of the simulation. The corresponding calculated force on the tank result is shown in **Figure 4**.

Figure 4 shows the absolute value of the force on the front, the rear wall of the tank, and the baffles. Actually, during the deceleration process, the force on the front wall, the rear side of baffles 1 and 2 have opposite directions of the other walls. During the acceleration and deceleration process, the force on the wall has the opposite direction. Therefore, the direction of the force is ignored during the analysis. During the deceleration process, the rear wall and rear side of baffle 2 have the maximum forces; the maximum forces occur during 0.35–0.6 s. The details of fluid distribution and pressure on the tank are shown in **Table 1**.

According to the work of Wenyuan Wang et al., the T-shaped baffle (as shown in **Figure 5**) is set in the tank to lower the movement of the fluid in the transverse direction (Wang et al., 2016). Based on the concept, the design of the baffle in the tank is provided, as shown in **Figure 6**; the cross section is shown in **Figure 7**. Normally, the pressure of the tank is taken as the anti-sloshing performance indicator; the lower pressure means the better performance. The improvement of the anti-sloshing capability may increase the weight of the tank. Thus, the pressure and anti-sloshing baffle weight are taken as the objectives while the four geometry parameters in **Figure 7** are chosen as the variables to be optimized.

For conflict objectives, multi-objective optimization is usually used to find the optimal parameter solution. In this case, it takes about 12.5 h to calculate the fluid movement in the tank with a workstation equipped with an E5-1620 V4 CPU. It is impossible to initiate each combination during the parameter optimization. Therefore, to optimize the tank parameters more efficiently, the approximation model is necessary to save computation time.

TABLE 3 | Variables range.

Variables	Define	Current value	Lower limit	Up limit
a	The minor axis of the ellipse	250	250	500
b	The major axis of the ellipse	250	250	800
y	Transverse offset distance	100	0	200
l	Longitudinal distance	0	0	400

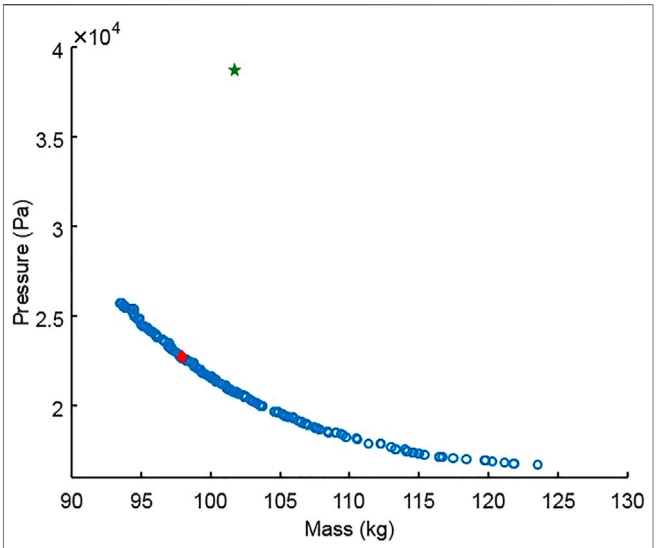

FIGURE 9 | Pareto front of the optimization.

APPROXIMATION MODEL

The approximation model is an approximation of the simulation result; it is widely used to build a simpler model with a lower computational cost. During this method, the internal behavior of the original simulation does not need to be understood; only the input and output are important (Díaz-Manríquez et al., 2016). Normally, three major steps are necessary to build an approximation model. First, some limited sampling points should be chosen, and the corresponding response of these points is calculated by the original model. With these data points, some techniques, such as rational functions, response surface method (Narendran and Karthikeyan, 2020), radial basis functions, Kriging models, polynomial regression, splines, and support vector machines, can be initiated to build the approximation model. At last, the accuracy of the approximation model should be validated before further analysis.

Design of the experiment

During the design of the experiment (DOE) process, the sampling points are selected with the optimal Latin hypercube design (OLHD). The advantage of this method is that it distributes the sampling points evenly by optimal conditions (Baek and Lee, 2020). Compared to the Latin hypercube design, it has improved projection properties and spatial fill properties. According to the OLED, the 60 sample points are distributed evenly without overlapping points. With the distributed variable points, 60 CFD models are built and simulated to gain the corresponding objective value. With the 60 groups' objective value and variable, the relationship between the objective and variables can be established by the Kriging method.

Kriging model

The typical form of the Kriging model can be expressed as follows (Simpson et al., 2001; Yu et al., 2020):

$$y(x) = g(x) + Z(x). \tag{10}$$

Here, $y(x)$ represents an unknown prediction function, $g(x)$ is a known approximate function, and $Z(x)$ means the realization of a stochastic process with a zero mean and nonzero covariance σ^2. In the covariance matrix $Z(x)$, the $(i, j)^{\text{th}}$ element is given as

$$Cov\left[Z(x_i), Z\left(x_j\right)\right] = \sigma^2 R\left(R\left[X_i, X_j\right]\right). \tag{11}$$

In the above equation, R represents the correlation function between the data points X_i and X_j. Usually, a Gaussian function is used as the correlation function, which is defined by

$$R\left(X_i, X_j\right) = \exp\left\{-\sum_{k=1}^{n}\theta_k\left(x_{ik} - x_{jk}\right)^2\right\}, \tag{12}$$

where θ_k means the distinct for each dimension, and the unknown parameters in the above equation are gained by solving a nonlinear optimization problem. k is the number of the variable, and x_i and x_j means the k^{th} data points in X_i and X_j.

The predicted value at the unknown point can be expressed as follows:

$$\widehat{y} = f^T(X)\widehat{\beta} + r^T(X)R^{-1}\left(y - F\widehat{\beta}\right), \tag{13}$$

where $f^T(X) = [f_1(x), f_2(x), \ldots f_m(x)]$ is the regression basis function of the approximation model, $\beta = [\beta_1, \beta_2, \ldots \beta_m]^T$ is the matrix of the regression coefficient which needs to be determined, $r^T(X) = [R(x, x_1), R(x, x_2), \ldots R(x, x_n)]$ is the correlation vector of n sampling points and unknown point x, y is the predicted value of n sampling points, and F means the function matrix of the global approximation model at n sampling points.

$$\widehat{\beta} = \left(F^T R^{-1} F\right)^{-1} F^T R^{-1} y. \tag{14}$$

The estimated variance can be gained by

$$\widehat{\sigma}^2 = \frac{\left[\left(y - F\widehat{\beta}\right)^T R^{-1}\left(y - F\widehat{\beta}\right)\right]}{n}. \tag{15}$$

The maximum likelihood estimation (MLE) of the Kriging model can be expressed as

$$\max_{\theta_k > 0} \Phi(\theta_k) = -\frac{n\ln\left(\widehat{\sigma}^2\right) + \ln|R|}{2}. \tag{16}$$

The optimal fitted Kriging approximation model can be acquired by solving the unconstraint k dimensional nonlinear optimization equation.

Model validation

Normally, the coefficient of determination R^2, root mean square error RMSE, and maximum absolute percentage error MAPE are

TABLE 4 | Comparison of fluid distribution.

Time (s)	Current tank	Optimized tank
0.35	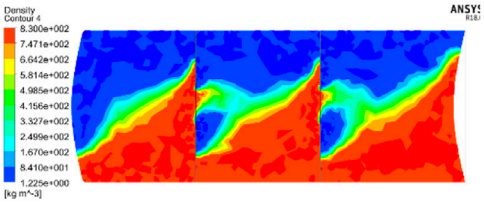	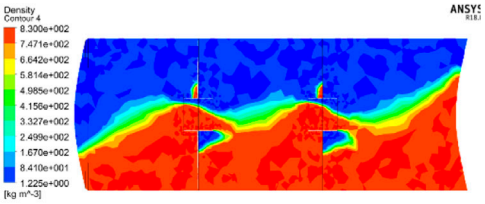
0.40	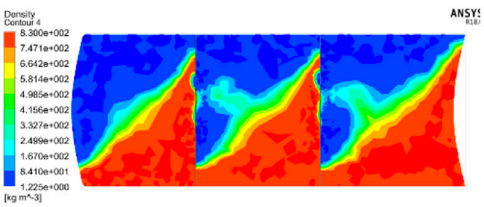	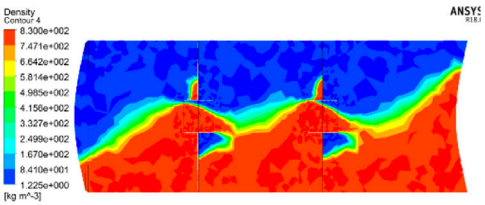
0.45	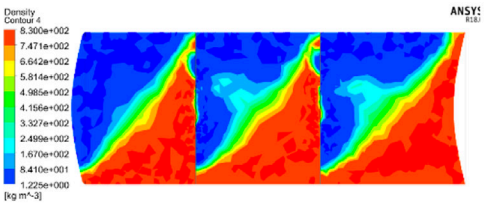	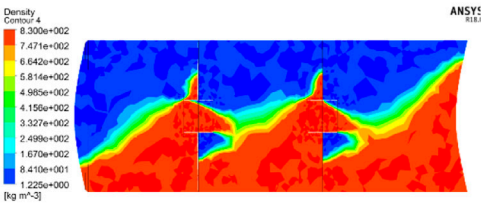
0.50	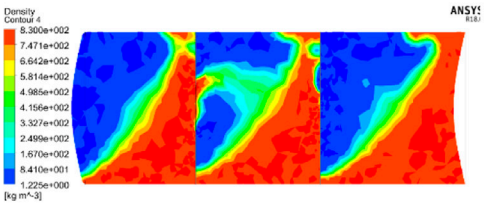	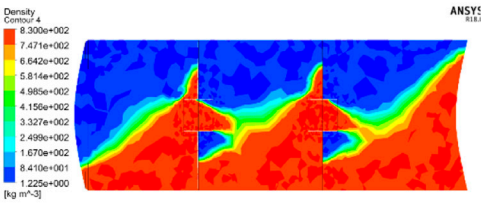
0.55	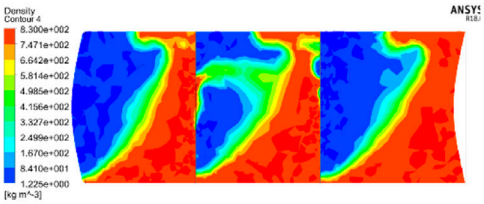	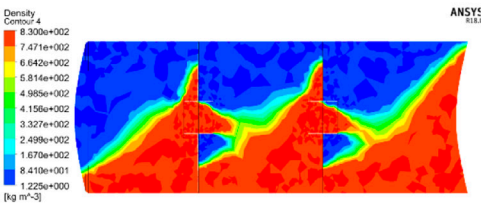
0.60	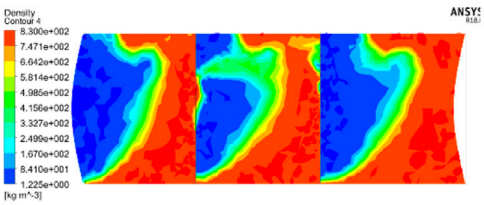	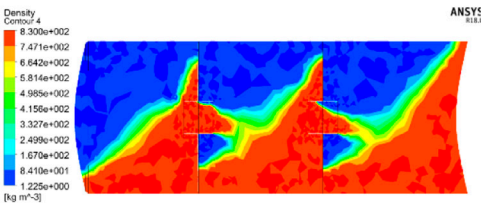

used to assess the accuracy of the approximation model. For R^2, the value close to 1 means better accuracy. For RSME and MAPE, the value close to 0 means better accuracy. These three indicators can be gained according to the following equations.

$$R^2 = \frac{\sum_{i=1}^{ntest}\left(\widehat{y}_i - \bar{y}\right)^2}{\sum_{i=1}^{ntest}\left(y_i - \bar{y}\right)^2}, \tag{17}$$

$$RMSE = \sqrt{\frac{1}{ntest}\sum_{i=1}^{ntest}\left(\widehat{y}_i - y_i\right)^2}, \tag{18}$$

$$MAPE = \max\left(\frac{\left|\widehat{y}_i - y_i\right|}{y_i}\right) \times 100\%, \tag{19}$$

where *ntest* means the number of test samples, and $\bar{y}$ is the mean value of the test result. According to the above equations and the

TABLE 5 | Comparison of pressure.

Time (s)	Current tank	Optimized tank
0.35	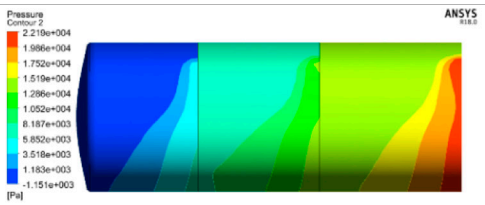	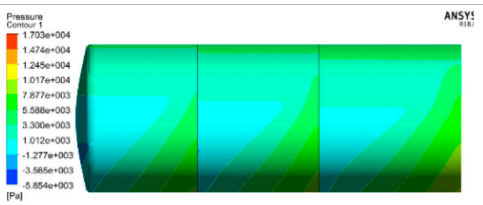
0.40	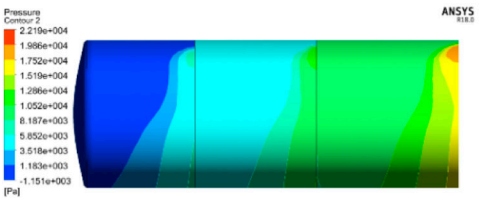	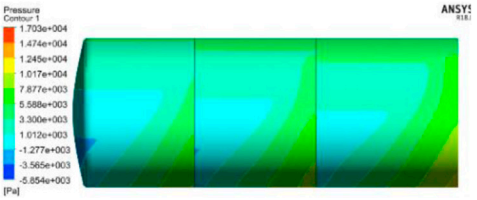
0.45	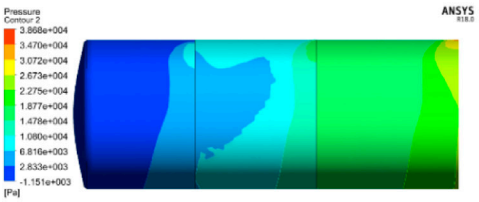	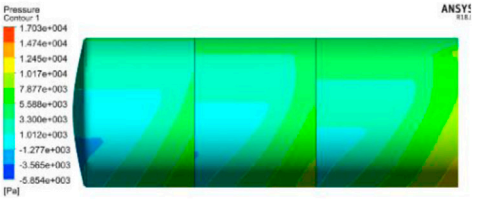
0.50	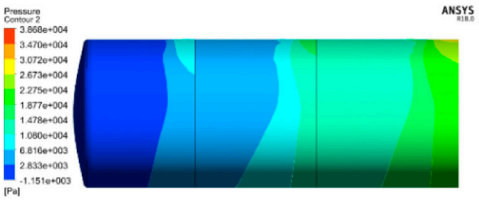	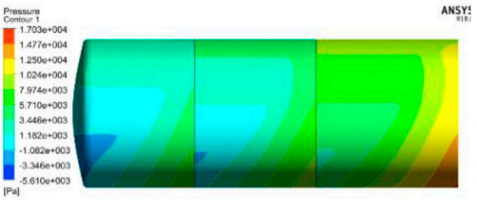
0.55	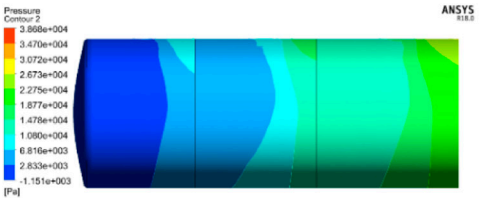	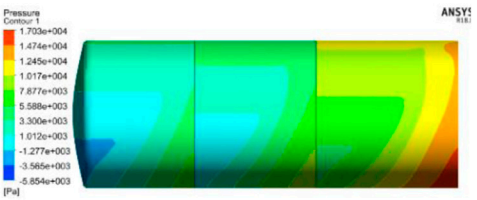
0.60	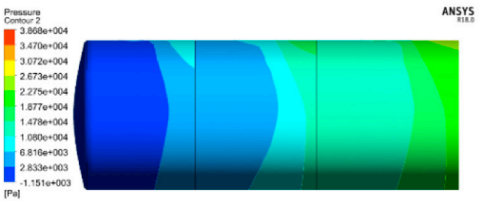	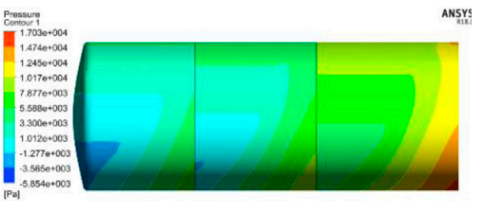

actual and predicted values, R^2, RMSE, and MAPE of the two objectives, pressure, and mass can be calculated, as shown in **Table 2**.

The error analysis in **Table 2** shows that the established Kriging model is accurate enough for further analysis.

MULTI-OBJECTIVE OPTIMIZATION

The NSGA-II approach, which is proposed by Deb et al. (Deb et al., 2002), is chosen to settle the multi-objective optimization problem. This method is based on the genetic algorithm with fast non-dominated sorting and crowded distance sorting methods to achieve Pareto solutions. It is widely used in the engineering area due to its advantages (Jiang et al., 2021), (Peng et al., 2021), (Li et al., 2021), (Zhang et al., 2021), (Li et al., 2020). The detail of NSGA-II is introduced in the study by Sedighizadeh et al., (2014). The optimization procedure of NSGA-II is presented in **Figure 8**.

According to the geometry space in the tank, the range of the variables can be determined, as shown in **Table 3**.

TABLE 6 | Objective of current and optimized tank.

Objective		Current tank	Optimized tank	Decreased percentage (%)
Baffle mass (kg)		101.74	98.92	2.77
Maximum pressure (Pa)		38,680	22,830	40.97
Wave damping time (s)		17.03	15.21	10.69
Maximum force (kN)	Front wall	12.78	9.52	34.24
	Front side of baffle 1	14.97	21.31	–29.75
	Rear side of baffle 1	11.18	21.58	–48.19
	Front side of baffle 2	19.37	22.59	–16.62
	Rear side of baffle 2	9.47	16.55	–42.78
	Rear wall	84.07	60.86	38.14

The Pareto front can be gained based on the above input. As shown in **Figure 9**, the mass of the anti-sloshing baffle and pressure caused by the moving fluid formed a curve with a different variable value. The green star means the initial value of the current anti-sloshing baffle; the red dot is chosen as the optimal result.

RESULTS AND DISCUSSION

The corresponding variable values of the optimal results a, b, y, and l are 328.95, 452.63, 115.79, and 126.31 mm. Considering the future manufacture, they are rounded as 329, 453, 116, and 126 mm, respectively. Based on these parameters, a CFD model is built and simulated. The comparison of the fluid distribution of the current tank and the tank with the optimized anti-sloshing baffle is shown in **Table 4**.

The comparison shows that the fluid movement after optimization is lower than before optimization, especially during 0.5–0.6 s. The T-shaped baffle can lower the fluid strike caused by truck deceleration. The decreased percentage can be identified by comparing the pressure and force on the tank. The pressure before and after optimization is compared in **Table 5**. The legend of each picture varies depending on the maximum pressure.

Besides the mass of baffles, maximum pressure, and force, the wave damping time after the shock caused by the acceleration and deceleration is also a vital indicator to judge the anti-sloshing performance of the baffle. The wave damping time means the period between the end of the shock, and the liquid is back to the original state.

The calculated mass of the baffles, maximum pressure, and force of the current tank and the tank with optimized baffles during the braking process are listed in **Table 6**.

According to the comparison in **Table 6**, with the optimized parameters, the baffle mass decreased with a percentage of 2.77%. The maximum pressure decreased with a dramatic percentage of 40.97%; the maximum force on the front and rear wall of the tank also decreased. The wave damping time of the oil also gets a reduction of 10.69%. Since the baffles bear with the sloshing liquid, the force on the baffles inside the tank increased. For the current tank, the maximum of the baffles and the front wall is much lower than the optimized tank. However, the work condition of the acceleration process is opposite to the deceleration process, which means, the maximum force on the front wall will be 84.07 kN, when the vehicle accelerates with the same acceleration. Therefore, during the strength design, the thickness of the front and rear walls should be the same, so does the baffles. For the tank with optimized parameters, the distribution of the force on the baffles, front, and rear wall are more even; thus, the thinner wall of the tank may be taken into consideration.

CONCLUSION

Based on the current analysis method and idea, a T-shaped baffle in the longitudinal direction is designed and optimized to lower the fluid movement in the tank during the brake process.

For the regular baffle, the baffles have a much lower force than the front and rear walls of the tank. Thus, the mass of the tank can be decreased by lowering the thickness of the baffles if only taking the acceleration (the maximum acceleration is lower than the maximum deceleration with the opposite direction) and deceleration work condition into consideration.

Compared to the regular baffle, the effect of the T-shaped baffle can decrease the force and pressure on the tank while the baffle inside the tank bears a bigger strike. The lower force and pressure caused by the moving fluid means the T-shaped anti-sloshing baffle can decrease the fluctuation of the fluid gravity center. Thus, the safety of the tank truck is improved.

DATA AVAILABILITY STATEMENT

The original contributions presented in the study are included in the article/Supplementary Material, further inquiries can be directed to the corresponding author.

AUTHOR CONTRIBUTIONS

YL was responsible for the manuscript and provided the original idea with BH. LZ and SZ finished the calculation task. BH provided the idea and was responsible for the correspondence.

FUNDING

This study was funded by the Innovative Research Team Development Program of Ministry of Education of China (IRT_17R83), and the 111 Project (B17034) of China.

REFERENCES

Akyıldız, H., Ünal, N. E., and Aksoy, H. (2013). An Experimental Investigation of the Effects of the Ring Baffles on Liquid Sloshing in a Rigid Cylindrical Tank. *Ocean Eng.* 59, 190–197.

Anderson, J. D., and Wendt, J. (1995). *Computational Fluid Dynamics*, 206. New York: McGraw-Hill, 332.

Baek, S.-W., and Lee, S. W. (2020). Design Optimization and Experimental Verification of Permanent Magnet Synchronous Motor Used in Electric Compressors in Electric Vehicles. *Appl. Sci.* 10 (9), 3235. doi:10.3390/app10093235

Belakroum, R., Kadja, M., Mai, T. H., and Maalouf, C. (2010). An Efficient Passive Technique for Reducing Sloshing in Rectangular Tanks Partially Filled with Liquid. *Mech. Res. Commun.* 37 (3), 341–346. doi:10.1016/j.mechrescom.2010.02.003

Deb, K., Pratap, A., Agarwal, S., and Meyarivan, T. (2002). A Fast and Elitist Multiobjective Genetic Algorithm: NSGA-II. *IEEE Trans. Evol. Computat.* 6 (2), 182–197. doi:10.1109/4235.996017

Díaz-Manríquez, A., Toscano, G., Barron-Zambrano, J. H., and Tello-Leal, E. (2016). A Review of Surrogate Assisted Multiobjective Evolutionary Algorithms. *Comput. intelligence Neurosci.* 2016. doi:10.1155/2016/9420460

Hasheminejad, S. M., Mohammadi, M. M., and Jarrahi, M. (2014). Liquid Sloshing in Partly-Filled Laterally-Excited Circular Tanks Equipped with Baffles. *J. Fluids Structures* 44, 97–114. doi:10.1016/j.jfluidstructs.2013.09.019

Hosseini, M., Goudarzi, M. A., and Soroor, A. (2017). Reduction of Seismic Sloshing in Floating Roof Liquid Storage Tanks by Using a Suspended Annular Baffle (SAB). *J. Fluids Structures* 71, 40–55. doi:10.1016/j.jfluidstructs.2017.02.008

Iranitalab, A., Khattak, A., and Bahouth, G. (2020). Statistical Modeling of Cargo Tank Truck Crashes: Rollover and Release of Hazardous Materials. *J. Saf. Res.* 74, 71–79. doi:10.1016/j.jsr.2020.04.010

Jiang, R., Jin, Z., Liu, D., and Wang, D. (2021). Multi-Objective Lightweight Optimization of Parameterized Suspension Components Based on NSGA-II Algorithm Coupling with Surrogate Model. *Machines* 9 (6), 107. doi:10.3390/machines9060107

Kolaei, A., Rakheja, S., and Richard, M. J. (2017). Coupled Multimodal Fluid-Vehicle Model for Analysis of Anti-slosh Effectiveness of Longitudinal Baffles in a Partially-Filled Tank Vehicle. *J. Fluids Structures* 70, 519–536. doi:10.1016/j.jfluidstructs.2017.02.012

Kolaei, A., Rakheja, S., and Richard, M. J. (2014). Effects of Tank Cross-Section on Dynamic Fluid Slosh Loads and Roll Stability of a Partly-Filled Tank Truck. *Eur. J. Mech. - B/Fluids* 46, 46–58. doi:10.1016/j.euromechflu.2014.01.008

Li, J., Khodayar, M. E., Wang, J., and Zhou, B. (2021). Data-driven Distributionally Robust Co-optimization of P2P Energy Trading and Network Operation for Interconnected Microgrids. *IEEE Trans. Smart Grid*. doi:10.1109/tsg.2021.3095509

Li, J., Liu, C., Khodayar, M. E., Wang, M.-H., Xu, Z., Zhou, B., et al. (2020). Distributed Online VAR Control for Unbalanced Distribution Networks with Photovoltaic Generation. *IEEE Trans. Smart Grid* 11 (6), 4760–4772. doi:10.1109/tsg.2020.2999363

Narendran, J., and Karthikeyan, T. (2020). Response Surface Methodology Based on Polyamide Incorporated with Biolubricant for Optimisation of Operating Parameters in Heavy Vehicles. *Int. J. Heavy Vehicle Syst.* Vol. 27, 97–125.

Noand Regulation, E. C. E. (2009). *Uniform Provisions Concerning the Approval of Vehicles of Categories M, N and O with Regard to Braking*, 13.

Liu, Zuoming (1999). *Road Vehicle-Braking Systems-Structure, Performance and Test Mehods*, 7.

Peng, D., Tan, G., Tang, J., and Guo, X. (2021). Design and Optimization of Forced-Air Cooling System for Commercial Vehicle Brake System. *SAE Int. J. Commercial Vehicles* 15.

Sanapala, V. S., M, R., Velusamy, K., and Patnaik, B. S. V. (2018). Numerical Simulation of Parametric Liquid Sloshing in a Horizontally Baffled Rectangular Container. *J. Fluids Structures* 76, 229–250. doi:10.1016/j.jfluidstructs.2017.10.001

Sedighizadeh, M., Faramarzi, H., Mahmoodi, M. M., and Sarvi, M. (2014). Hybrid Approach to FACTS Devices Allocation Using Multi-Objective Function with NSPSO and NSGA-II Algorithms in Fuzzy Framework. *Int. J. Electr. Power Energ. Syst.* 62, 586–598. doi:10.1016/j.ijepes.2014.04.058

Simpson, T. W., Mauery, T. M., Korte, J., and Mistree, F. (2001). Kriging Models for Global Approximation in Simulation-Based Multidisciplinary Design Optimization. *AIAA J.* 39 (12), 2233–2241. doi:10.2514/3.15017

Ünal, U. O., Bilici, G., and Akyıldız, H. (2019). Liquid Sloshing in a Two-Dimensional Rectangular Tank: A Numerical Investigation with a T-Shaped Baffle. *Ocean Eng.* 187, 106183. doi:10.1016/j.oceaneng.2019.106183

Wan, Yin. (2018). *Study on Vehicle-Liquid Coupling Dynamic Characteristics and Anti-rollover Control Method for Tank Vehicles*. China: Jilin University, MA.

Wan, Y., Zhao, W., Zong, C., Zheng, H., and Li, Z. (2019). Modeling and Analysis of the Influences of Various Liquid Sloshing Characteristics on Tank Truck Dynamics. *Int. J. heavy vehicle Syst.* 26 (3-4), 463–493. doi:10.1504/ijhvs.2019.101468

Wang, W., Guo, Z., Peng, Y., and Zhang, Q. (2016). A Numerical Study of the Effects of the T-Shaped Baffles on Liquid Sloshing in Horizontal Elliptical Tanks. *Ocean Eng.* 111, 543–568. doi:10.1016/j.oceaneng.2015.11.020

Xue, M.-A., and Lin, P. (2011). Numerical Study of Ring Baffle Effects on Reducing Violent Liquid Sloshing. *Comput. Fluids* 52, 116–129. doi:10.1016/j.compfluid.2011.09.006

Xue, M.-A., Zheng, J., Lin, P., and Yuan, X. (2017). Experimental Study on Vertical Baffles of Different Configurations in Suppressing Sloshing Pressure. *Ocean Eng.* 136, 178–189. doi:10.1016/j.oceaneng.2017.03.031

Yu, M., Li, X., and Liang, J. (2020). A Dynamic Surrogate-Assisted Evolutionary Algorithm Framework for Expensive Structural Optimization. *Struct. Multidisc Optim* 61 (2), 711–729. doi:10.1007/s00158-019-02391-8

Zhang, J., Wu, W., and Hu, J. (2016). A Numerical Study of the Effects of the Longitudinal Baffle on Nickel Ore Slurry Sloshing in a Prismatic Cargo Hold. *Mar. Structures* 46, 149–166. doi:10.1016/j.marstruc.2016.01.003

Zhang, K., Zhou, B., Or, S. W., Li, C., Chung, C. Y., and Voropai, N. I. (2021). Optimal Coordinated Control of Multi-Renewable-To-Hydrogen Production System for Hydrogen Fueling Stations. *IEEE Trans. Industry Appl.* doi:10.1109/tia.2021.3093841

Zhang, Z. L., Khalid, M. S. U., Long, T., Chang, J. Z., and Liu, M. B. (2020). Investigations on Sloshing Mitigation Using Elastic Baffles by Coupling Smoothed Finite Element Method and Decoupled Finite Particle Method. *J. Fluids Structures* 94, 102942. doi:10.1016/j.jfluidstructs.2020.102942

Conflict of Interest: LZ was employed by the Company Wuhan Road Rover Intelligent Technology Co., Ltd.

SZ was employed by the Company Liuzhou Wuling Automobile Industry Co., Ltd.

The remaining authors declare that the research was conducted in the absence of any commercial or financial relationships that could be construed as a potential conflict of interest.